Analytical Methods

PAPER

View Article Online
View Journal | View Issue

Cite this: *Anal. Methods*, 2015, 7, 5476

Detection of orchid viruses by analyzing Brownian diffusion of nanobeads and virus–immunobead association

Yu-Jui Fan,[a] Ya-Chun Chang,*[b] Chao-Ti Teng,[a] Ting-Ya Liao,[a] Wen-Chi Hu[b] and Horn-Jiunn Sheen*[a]

Received 5th March 2015
Accepted 21st May 2015

DOI: 10.1039/c5ay00577a

www.rsc.org/methods

This paper describes a new sensing technique for detecting orchid viruses by measuring the Brownian diffusion of immunobeads in liquid samples. Both the capsid proteins and virus particles of *Odontoglossum ringspot virus* (ORSV) are detectable targets by using this technique. When the targets bind to immunobeads, the Brownian diffusion of the beads decreases. Thereafter, the kinetic model of the antibody–antigen interaction in a free liquid space can be established. This model is used to calculate the association constant rate, dissociation constant rate, and dissociation constant of ORSV capsid proteins and antibody-coated nanobeads. This paper presents the results of using 300 nm immunobeads to detect ORSV capsid proteins and particles in a phosphate-buffered saline solution, as well as the results of using 500 nm beads to detect ORSV particles in a plant sap solution. In addition, transmission electron microscopy images of the antibody-coated nanobeads reacting to low and high concentrations of the ORSV are shown.

Introduction

Immunoassays are normally used to quantify the biological targets of interest and are widely used in many important areas such as diagnosis of diseases, therapeutic drug monitoring, clinical pharmacokinetic and bioequivalence studies in drug discovery, and pharmaceutical industries.[1] The sensitivity and reaction rate are highly related to the antibody–antigen specificity, reaction area, and the rate of physical collision. The conventional immunoassay methods require a sensing region to modify the ligands. The detection zone is a fixed two-dimensional (2D) region, so that the probability of antibody–antigen collision and the number of captured targets are highly limited.

Recently, micro/nanobeads have been used for immunoassays by modifying the ligand on the spherical surface to interact with the targets. Compared with a traditional immunoassay, immunobeads provide a three-dimensional (3D) interaction environment and substantially increase the reaction area for target detection and probability of the antibody–antigen collision.

Immunobeads have been used for many purposes including the determination of the incidence of sperm-bound antibodies,[2] detection of ciguatoxin on cell membranes,[3] multiple analyses of cytokines in human serum,[4–6] detection of cancer biomarkers in saliva,[7] and detection of tacrolimus.[8] The challenge of an immunobead assay is to quantify analytes captured on immunobeads. Several approaches have been developed to extract immunobeads and/or quantify analytes, such as ELISA,[7] collection of magnetic immunobeads for PCR,[9,10] collection of magnetic immunobeads for chemiluminescence,[11] enzyme-based electrochemical immunoassay,[12] collection and quantification of immunobeads by using a microfluidic channel structure,[8] and quantification of immunobeads by flow cytometery.[13] However, these approaches normally require complex processes and may not be suitable for system integration.

To simplify the capturing and quantification of analytes by performing the immunobead assay, the ligand-coated nanobeads were suspended in a sample solution and then the variation in Brownian diffusion of nanobeads was measured to quantify analytes.[14–17] The biomolecule detection method involving the direct measurement of nanobead diffusion demonstrates high sensitivity and uses nanoliters of samples. Compared with other transducer mechanisms, the present method shows substantial potential to integrate with a microfluidic device because the measurement of nanobead diffusion does not require a micro-structure through micro-fabrication.

This study reports the orchid virus quantification by statistically analyzing the time-dependent variation in the Brownian diffusion of nanobeads as shown in Fig. 1. Among the various orchids, *Phalaenopsis* and *Oncidium* are two major orchid genera, cultivated by commercial growers in Taiwan.[18] More than 50 viruses have been reported to infect orchids in various regions of the world, and the *Cymbidium mosaic virus* (CymMV) and *Odontoglossum ringspot virus* (ORSV) are the most prevalent

[a]*Institute of Applied Mechanics, National Taiwan University, No. 1, Sec. 4, Roosevelt Road, Taipei, 10617 Taiwan. E-mail: sheenh@ntu.edu.tw*
[b]*Department of Plant Pathology and Microbiology, National Taiwan University, No. 1, Sec. 4, Roosevelt Road, Taipei, 10617 Taiwan. E-mail: ycchang@ntu.edu.tw*

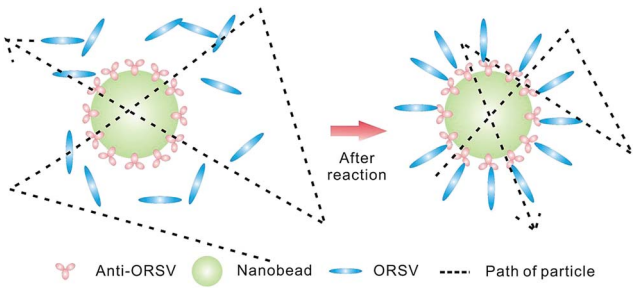

Fig. 1 Schematics of the sensing mechanism. After ORSV binding, the Brownian displacement of anti-ORSV coated nanobeads is decreased.

and economically important viruses.[19–21] Because of their worldwide occurrence and their ability to induce obvious symptoms, CymMV and ORSV can infect several orchid genera, often reducing the vigor of plants and lowering the quality of flowers. However, the leaves of some orchid cultivars appear normal even when infected with these two viruses.[19]

We firstly demonstrated the ORSV sensing. The anti-ORSV IgG-modified nanobeads were suspended in a solution prepared using ORSV particles and/or capsid proteins. The nanobeads in different concentrations of ORSV particles/capsid proteins exhibited variations in Brownian diffusion. In the detectable range, a high concentration of the ORSV was related to a large variation in the Brownian velocity of the nanobeads. When the concentration of the ORSV reached a saturation point, the decaying curves of the Brownian velocities of the nanobeads in different concentrations almost overlapped. Based on the results of the anti-ORSV IgG-coated nanobead-sensing of ORSV capsid proteins, we developed a new kinetic association model to analyze the anti-ORSV IgG and ORSV interaction in a 3D free liquid space. The sensing results of the ORSV particles in pure phosphate-buffered saline (PBS) solution and leaf sap prepared by PBS were investigated.

Experimental section

Preparation

Testing sample. *Phalaenopsis* orchids collected from growers were verified as healthy or infected with the ORSV by ELISA using the ORSV antibody.[2] The ORSV isolated from the orchids was maintained in tobacco (*Nicotiana benthamiana*) plants for virion purification. These plants were kept in a greenhouse with day and night temperatures of 28 °C and 25 °C and for 16 h and 8 h, respectively, at the National Taiwan University. Virus particles were purified from ORSV-infected tissues according to the method described by Chapman[22] and treated as experimental standards.

Healthy plant sap was prepared by grinding healthy leaves with 10 volumes of PBS (1 : 10, w : v). For sample preparation, different amounts of ORSV particles or capsid proteins were added into healthy plant sap to mimic the infected samples containing different concentrations of viruses.

Antibody modification on nanobeads. Polystyrene beads with diameters of 300 nm (Merck™ XC030) and 500 nm (Merck™ XC050), which are observable sizes of particles in our system, were used. The optimal excitation and emission wavelengths of these nanobeads were 475 nm and 525 nm, respectively. The nanobeads were modified to bind with a carboxyl functional group ($COOH^-$) at their surface for coupling ORSV antibodies on the nanobead surface through the standard ethyl(dimethylaminopropyl)carbodiimide/*N*-hydroxysuccinimide (EDC/NHS) crosslinking protocol.[23] A sonicator and several types of porous membrane filters with different aperture sizes were used to reduce self-assembly of beads and filter bead clusters. Reactors for antibody-coated nanobeads and antigen interactions were manufactured using a simple polydimethylsiloxane (PDMS) fabrication process that involves patterning of a thick photoresist (SU-8 2050) on a silicon wafer as a mold, pouring PDMS into the mold, and subsequently baking the PDMS. The depth and diameter of the microchambers were 40 μm and 12 mm, respectively.

Theory

Brownian diffusion. Brownian diffusion, which is the random motion of particles suspended in a liquid, results from the collision of atoms, molecules, and particles. In 1905, Albert Einstein statistically explained the probability distribution of the particle motion (p) in a 2D environment and derived the ensemble average of the particle motion[24] as follows:

$$p(x, y, t) = \langle x_p^2 + y_p^2 \rangle = 4Dt \quad (1)$$

where t is the time. The diffusion coefficient D is given as follows:

$$D = \alpha \frac{kT}{3\pi\mu d_p} \quad (2)$$

where k is the Boltzmann constant, $k = 1.3805 \times 10^{-23}$ J K^{-1}, T is the absolute temperature of the fluid, μ is the solvent viscosity, and d_p is the particle diameter. Assuming that the temperature and viscosity are constants, when the antigen and the antibody interact, the particle diameter will increase and the diffusion coefficient of the particle will decrease. The measurement results showed that as the number of antigens conjugating with antibody-coated nanobeads increased, the Brownian diffusion of nanobeads decreased.

Micro-particle tracking velocimetry. A micro-particle tracking velocimetry (micro-PTV) method was employed to statistically analyze the variation in the Brownian velocity of nanobead population in a specific time-interval. The liquid sample containing fluorescent nanobeads was loaded on an inverted microscope with a 20× objective lens with a numerical aperture of 0.7. A 3D random movement of the nanobeads was projected onto a charge-coupled device (CCD) camera and 2D images of the nanobeads were captured. A time-resolved imaging system was used to analyze the mean displacements and the standard deviations of the nanobeads in a specific time.

Micro-PTV is a powerful method for particle movement analysis by using sequential images. A programmable CCD camera, which can control the time interval between each image pair, was used to recognize and trace the trajectory of the

fluorescent nanobeads. The position of each nanobead in an image was identified and recorded based on the intensity and size of the nanobeads. By comparing the position of particles between each image pair, the displacement of each particle was calculated; furthermore, the standard deviation of nanobead population between image pairs was calculated and considered as the Brownian velocity of the nanobeads. The variations in the Brownian velocity of nanobeads with time can be determined by analyzing sequential image pairs. By employing micro-PTV, the probability distribution of the nanobead velocity can be obtained using the following modified equation:

$$p(V_x,\ V_y,\ t) = \left\langle {V_{x,\mathrm{p}}}^2 + {V_{y,\mathrm{p}}}^2 \right\rangle = \frac{4D}{t} \tag{3}$$

where V_x and V_y are the nanobead velocities in x and y directions. In this study, the probability distributions of particle velocities are designated as Brownian velocities.

Kinetic association model. We assumed that the two combining sites of a bivalent antibody, anti-ORSV IgG, are equivalent and that neither was affected by the other. Therefore, the anti-ORSV IgG can be considered as a monovalent molecule. The antibody (anti-ORSV IgG, B) was immobilized on the nanobeads suspended in a free liquid space, and the antigen (ORSV capsid protein, A) was transported by diffusion and random collision to the nanobeads. The formation of a surface-bound complex (AB) on the nanobead surface is a three-step process. First, the capsid protein travels a distance from the liquid space to the bead surface. Second, the antibody and antigen rotate to an appropriate orientation for the reaction. Finally, a complexation process occurs:

$$\mathrm{A_{bulk}} \underset{k_\mathrm{m}}{\overset{k_\mathrm{m}}{\rightleftharpoons}} \mathrm{A_{surface}} + \mathrm{B} \underset{k_\mathrm{d}}{\overset{k_\mathrm{a}}{\rightleftharpoons}} \mathrm{AB} \tag{4}$$

where k_m is the rate constant for mass transport to and from the bead's surface. Furthermore, the rate constants of mass transport for the forward and backward directions are similar. For the AB complex, k_a and k_d are the rate constants for the formation and degradation, respectively. The equilibrium equation and its reaction rate for complex formation may be written as follows:

$$\mathrm{A_{bulk}} + \mathrm{B} \underset{k_\mathrm{r}}{\overset{k_\mathrm{f}}{\rightleftharpoons}} \mathrm{AB}, \tag{5}$$

and

$$\frac{\mathrm{d[AB]}}{\mathrm{d}t} = k_\mathrm{f}[\mathrm{A_{bulk}}][\mathrm{B}] - k_\mathrm{r}[\mathrm{AB}] \tag{6}$$

where k_f and k_r are the measured effective forward and reverse rate constants, respectively, according to Glaser *et al.*[25]

$$\begin{aligned} k_\mathrm{f} &= \frac{k_\mathrm{a}k_\mathrm{m}}{k_\mathrm{a}[\mathrm{B}] + k_\mathrm{m}} = \frac{k_\mathrm{a}}{1 + k_\mathrm{a}[\mathrm{B}]/k_\mathrm{m}} \\ k_\mathrm{r} &= \frac{k_\mathrm{d}k_\mathrm{m}}{k_\mathrm{a}[\mathrm{B}] + k_\mathrm{m}} = \frac{k_\mathrm{d}}{1 + k_\mathrm{a}[\mathrm{B}]/k_\mathrm{m}} \end{aligned} \tag{7}$$

If the mass transport rate (k_m) from the bulk solution to the surface is substantially faster than the interaction-controlled association rate (k_a[B]), the term $1 + k_\mathrm{a}[\mathrm{B}]/k_\mathrm{m}$ is approximated to one, and the measured forward (k_f) and backward (k_r) rate constants are approximated to the association (k_a) and dissociation (k_d) rate constants, respectively. Therefore, the antigen concentration at the surface [$\mathrm{A_{surface}}$], which is maintained at the same concentration as that in the bulk phase [$\mathrm{A_{bulk}}$], can be obtained. Based on these conditions, the rate equation can be rewritten as follows:

$$\frac{\mathrm{d[AB]}}{\mathrm{d}t} = k_\mathrm{a}[\mathrm{A}][\mathrm{B}] - k_\mathrm{d}[\mathrm{AB}] \tag{8}$$

The concentration of the unoccupied antibody epitopes [B] is the difference between the total amount of the antibody epitopes on the surface $[\mathrm{B}]_\mathrm{o}$ and the amount of the complex [AB]:

$$[\mathrm{B}] = [\mathrm{B}]_\mathrm{o} - [\mathrm{AB}] \tag{9}$$

Because the immunobeads are much larger than the antigens, we assumed that the variation of [AB] is linearly increased with the nanobeads' diameter. Based on eqn (2), the diffusion coefficient is also related to the variation of [AB]. Here, we used R to represent the Brownian velocity of nanobead population Thus, an increase in the antibody–antigen interaction resulted in an increase in the amount of the complex [AB] and a decrease in the Brownian velocity (R) of the nanobeads. When the total amount of ligands on the occupied surface increased, Brownian diffusion was the lowest and can be expressed as R_min. This indicated that the total amount of unoccupied ligands can be expressed as $R - R_\mathrm{min}$. Therefore, the formation rate of a complex molecule is quantified and presented as follows:

$$\frac{\mathrm{d}R}{\mathrm{d}t} = k_\mathrm{a}C(R - R_\mathrm{min}) - k_\mathrm{d}R \quad \text{when} \quad \frac{\mathrm{d}R}{\mathrm{d}t} < 0, \tag{10}$$

where $\mathrm{d}R/\mathrm{d}t$ is the rate of change in the binding signal, k_a is the association rate constant, C is the analyte (ORSV capsid protein) concentration, and k_d is the dissociation rate constant. Based on the measurement of Brownian diffusion, the Brownian velocities R decreased as the analytes bound onto the antibody-coated nanobeads; thus, $\mathrm{d}R/\mathrm{d}t$ was negative. To estimate the reaction constant by using this kinetic association model, eqn (10) is rearranged as follows:

$$\frac{\mathrm{d}R}{\mathrm{d}t} = (k_\mathrm{a}C - k_\mathrm{d})R - k_\mathrm{a}CR_\mathrm{min} \tag{11}$$

This equation clearly indicates a linear relationship between $\mathrm{d}R/\mathrm{d}t$ and R, with slope S, which can be derived as follows:

$$S = k_\mathrm{a}C - k_\mathrm{d} \tag{12}$$

Therefore, by using the linear regression method based on the relationship between S and concentration C of the capsid, k_a and k_d can be obtained. Furthermore, the results can be used to determine the dissociation constant K_D:

$$K_\mathrm{D} = \frac{k_\mathrm{d}}{k_\mathrm{a}} \tag{13}$$

Results and discussion

Capsid protein sensing

We conducted an experiment to clarify the interaction between ORSV capsid proteins and ORSV antibodies by using 300 nm beads in PBS with different ORSV capsid protein concentrations of 0, 0.1, 0.2, 0.4, 0.8, 1.2, 2, 4, 8, 16, and 32 μg mL^{-1}. The prepared antibody-coated nanobeads were thoroughly mixed with each pretreated ORSV capsid protein solution, and the mixture was injected into a microchamber and incubated for 180 s before micro-PTV measurements. The variations in the Brownian velocities for different concentration solutions are shown in Fig. 2. The results showed that the equilibrium states of the different concentration samples were attained in 800 s. The values of the Brownian velocities at equilibrium states are shown in Fig. 3. At equilibrium, a reasonable linear detection range of 0.1–2 μg mL^{-1} can be experimentally demonstrated as shown in the inset of Fig. 3. When the concentrations of the test samples were equal to or more than 4 μg mL^{-1}, the fitting variation curves almost overlapped (Fig. 2b), which meant that the analyte (ORSV capsid protein) concentration was saturated. In the detectable region, the Brownian velocity of the nanobeads proportionally decreased as the concentration of the capsid protein increased. When the concentration of the capsid protein was more than 4 μg mL^{-1}, the Brownian velocities of the nanobeads increased because of two reasons: (a) the binding regions of the nanobeads were saturated and (b) the unbound proteins might affect the neighboring nanobeads.

Kinetic association analysis

The inset in Fig. 3 shows that the usable analyte concentrations are in the range of 0.1–2 μg mL^{-1}, in which the slope linearly decreased. Hence, we selected the linear regime of concentration variations to analyze the kinetic association. Based on eqn (11), a plot of dR/dt against R is theoretically a straight line with a slope of $k_aC - k_d$, as shown in Fig. 4a for interaction-controlled kinetics. At the initial state of the interaction, the binding rate is directly proportional to the antigen (ORSV capsid protein) concentration. Fig. 2 shows the measurement of the association sensorgram at different capsid protein concentrations. To analyze the on and off rates, k_a and k_d, dR/dt was plotted against R at different capsid protein concentrations C to produce the value of slope S, which associated the on and off rates according to eqn (12). Subsequently, $k_a = 2 \times 10^5$ and $k_d = 2.67 \times 10^{-2}$ were calculated using the slope S and the intercept of the linear regression of S *versus* C, according to eqn (12) and as shown in Fig. 4b. The concentration unit was changed to the molar concentration based on the molecular mass of the ORSV capsid protein, which was 17.727 kDa.[26] Therefore, the corresponding dissociation constant $K_D = 1.33 \times 10^{-7}$ M was calculated using eqn (13). In addition, a maximum detectable concentration of 2.44 μg mL^{-1} was obtained.

The dissociation constant is a specific equilibrium constant that measures the propensity of a compound object (*e.g.*, antibody–antigen complex) to separate reversibly into antibody and antigen components. The dissociation constant is the inverse of the association constant, which is a specific equilibrium constant that measures the antibody–antigen interaction. The association model that we developed was useful for analyzing antigen binding onto immunobeads.

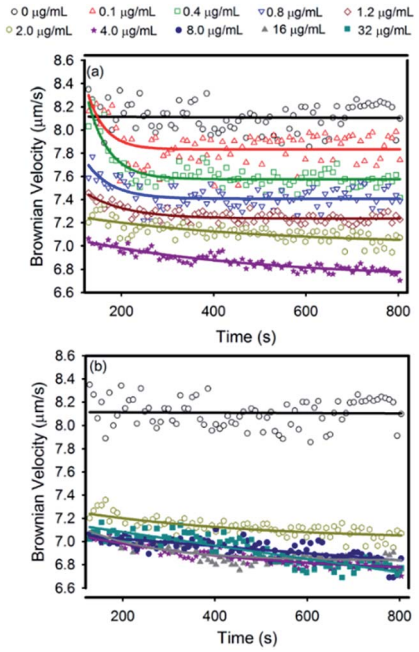

Fig. 2 *In situ* Brownian velocity variations of the anti-ORSV IgG coated 300 nm beads in different ORSV capsid protein concentrations. When the capsid proteins' concentrations are equal to or higher than 4 μg mL^{-1}, the decay curves of the variations are almost overlapped.

Odontoglossum ringspot virus particle sensing

We demonstrated ORSV particle sensing by employing the Brownian motion sensing technique. The antibody-coated 300 nm nanobeads were used for sensing an ORSV particle, which is rigid rod-shaped, 18 nm in diameter, and 300 nm in

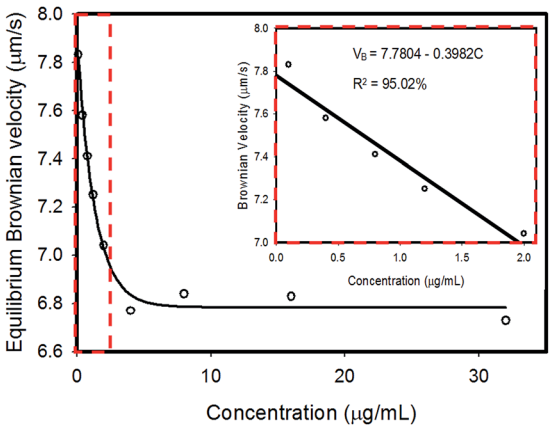

Fig. 3 After reacting with different concentrations of ORSV capsid proteins, the values of nanobeads' Brownian diffusions at the equilibrium state show a linear decrease in the concentration range of 0.1–2 μg mL^{-1}.

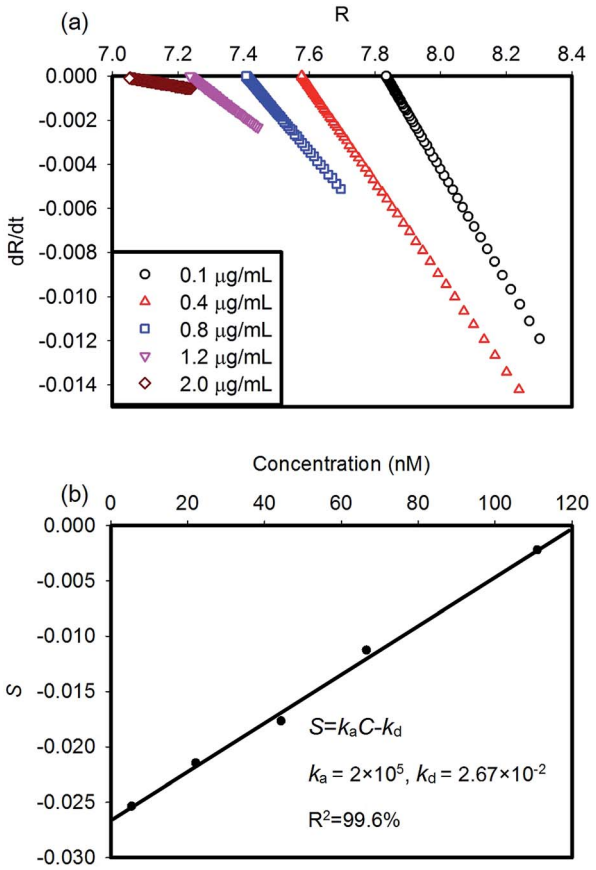

Fig. 4 (a) The results of linear regressions of d*R*/d*t* and *R* for eqn (11) and (b) the plot of *S versus C* for eqn (12).

length.[27] We prepared ORSV particle solutions at concentrations of 0, 0.8, 2, 4, and 8 μg mL^{-1} in PBS, and then mixed the solutions with antibody-coated nanobeads when performing sensing examinations. The results of real-time variations in the Brownian velocity at different concentrations are shown in Fig. 5. Based on the results, the decay range of sensing ORSV particles was substantially wider than that of sensing ORSV capsid proteins; this was because the size of ORSV particles bound onto nanobeads was larger than that of capsid proteins. Furthermore, the saturated concentration of ORSV particles was approximately 4 μg mL^{-1}, which was similar to that obtained while sensing capsid proteins.

In addition, we detected ORSV particles in plant sap by measuring the Brownian diffusion of nanobeads. In the experiments, 500 nm antibody-coated nanobeads were used instead of 300 nm beads. Compared with the 300 nm beads, the 500 nm nanobeads provided more surface area and binding sites to bind more targets. The test samples were prepared by mixing ORSV particles with the plant sap solution at concentrations of 0, 0.1, 0.8, 2, 4, and 8 μg mL^{-1}. For sensing experiments, the antibody-coated nanobeads were added into the test samples and injected into the reaction chamber after thorough mixing. Fig. 6 shows the results of variations in the Brownian velocity of the nanobeads in ORSV particle samples with different concentrations at a specific time-interval. The detectable

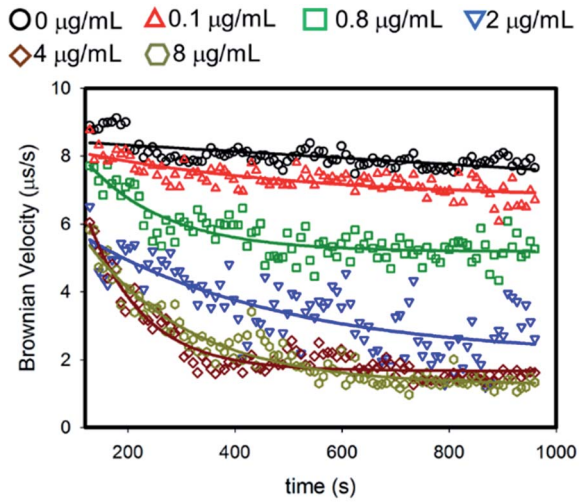

Fig. 5 Detection of ORSV particles with different concentrations using 300 nm beads.

concentration range of 0.1–4 μg mL^{-1} was obtained, which was similar to that obtained using 300 nm beads for ORSV particle and capsid protein detection. Compared with the variation in the detectable range obtained using the 300 nm beads, the variation in the detectable range obtained using 500 nm beads was narrow. However, the initial values of Brownian velocities for the 500 nm and 300 nm beads were similar because the crude plant sap in which the 500 nm beads were suspended contained many non-targeted containments. The contaminents suspended in the samples increased the possibility of particle–particle collision; consequently, the Brownian velocities increased.

Our experimental results show that using 300 nm beads will have larger variations of the Brownian velocity than those using 500 nm beads. We can conclude that the smaller particles will have larger size variations when conjugated with the targets,

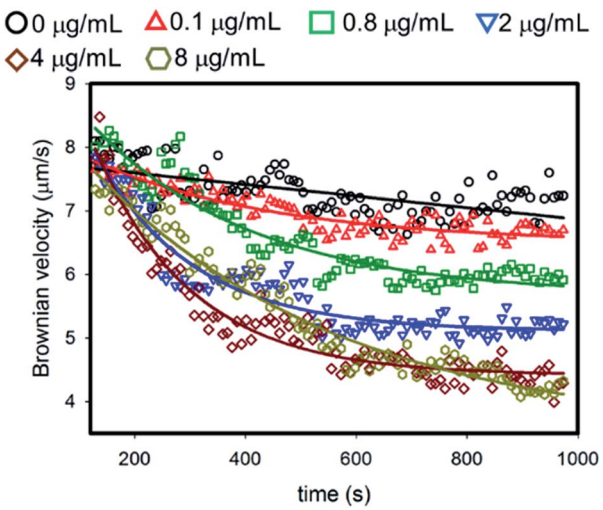

Fig. 6 Detection of ORSV particles in plant sap with different concentrations using 500 nm beads.

ORSV. This phenomenon leads to the fact that the Brownian velocity variations of using smaller particles before/after target binding will be more pronounced. Furthermore, our results also show that the assays using 300 nm immunobeads reached the equilibrium state faster than that using 500 nm immunobeads. On the other hand, the 500 nm beads provided more ORSV conjugation for higher concentration detection rather than using 300 nm beads.

From Figs. 2, 5 and 6, the detection results of the capsid proteins and ORSV particles reveal that the statistical data show large deviations. We conclude that these may be contributed by particle size variation, non-specific binding to the particles, and heat fluctuations from the environment. Although the original diameters of the nanobeads are not uniform and given as 299 ± 6 nm and 506 ± 6 nm as shown in the Merck™ package, in our study, we observed the same one group of nanobeads in each ORSV detection experiment. We concluded that the large deviation is not contributed from the original particle size variation.

We believed that the particle size variation may not be the major contributor for velocity deviation. Instead, the non-specific binding is regarded as the major factor for the deviation. However, the statistical data of the detection results in PBS show similar deviations to the results in leaf sap. Further, the non-conjugated sites of the nanobeads are quenched, the results lead to the fact that the non-specific bindings were dramatically reduced. For heat fluctuations, the samples were isolated in a PDMS chamber and glass substrate. The temperature of the samples cannot be directly measured. However, the temperature fluctuations outside the PDMS chamber were monitored to be within 1 °C, and it may contribute to the variation of the statistical results.

To verify the conjugation of the ORSV with anti-ORSV IgG-coated nanobeads, a transmission electron microscope (TEM) was used to capture the images of nanobeads when reacting with the ORSV. For TEM imaging, the samples containing ORSV-reacted nanobeads were negatively stained with 3% phosphotungstic acid and examined in a field emission microscope (Jeol, JEM-1400). The TEM images shown in Fig. 7 suggest that a notable fraction of the ORSV extended at full length from the nanobeads. When the ORSV completely occupied the surface of the nanobead as shown in Fig. 7b, the diameter of the nanobead increased from 500 nm to 1100 nm, which is an average increase of 600 nm. From the TEM images, we can conclude that the reasons for the decrease in Brownian velocity include an increase in the size of nanobeads and an increase in the form drag of the nanobeads. However, the present kinetic model, which was developed under the assumption that nanobeads uniformly increase in size during target binding, cannot be applied for sensing ORSV particles.

We also measured the Brownian velocity of 500 nm immunobeads suspended in the sample of the ORSV-infected orchid leaf. The infection of the leaf was validated by ELISA testing. The results were also compared with the fitting curves in Fig. 6 and plotted in Fig. 8a. From this figure, we found that the decay curve of the Brownian velocity of the immunobeads was located in-between the concentration of 0.1 and 0.8 μg mL^{-1}. Fig. 8b shows the fitting curve of the Brownian velocity at the equilibrium state of the immunobeads in different ORSV concentrations. Thus, the ORSV concentration of the sample can be estimated when the immunobeads' Brownian velocity is obtained.

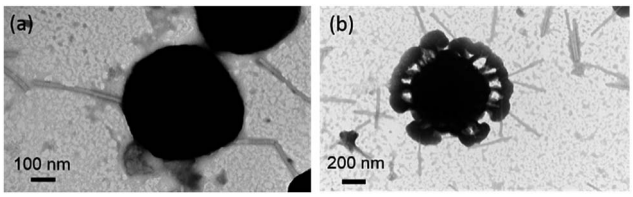

Fig. 7 TEM images show that the nanobeads conjugate with the ORSV when the nanobeads are suspended in (a) low- and (b) high-concentration of ORSV samples. The phosphotungstic acid dye will accumulate at the location of complex structures, so that it looks like a broccoli when the ORSV fully covers the nanobead surface.

The anti-ORSV IgG-modified 300 nm beads suspended in PBS and stored at 4 °C for 0, 3, and 12 months were tested. These nanobeads reacted with solutions containing 4 μg mL^{-1} of ORSV particles and were compared with the control sample (fresh antibody-coated nanobeads without the antigen reaction). Fig. 9 shows that when the anti-ORSV-modified beads

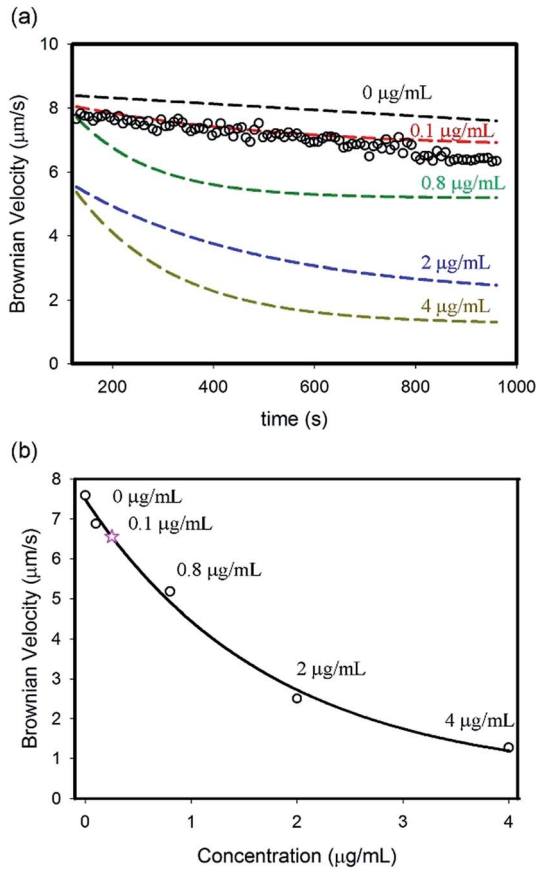

Fig. 8 Detection of ORSV particles in ORSV-infected leaf sample assay. (a) The variation of the Brownian velocity of the nanobeads, and (b) the Brownian velocity of the nanobeads at the equilibrium state, comparing with the fitting curves of different ORSV concentration assays shown in Fig. 6.

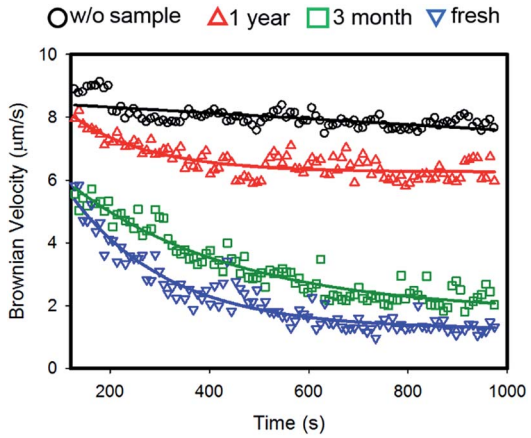

Fig. 9 The storage life test of anti-ORSV modified nanobeads.

were stored for 3 months, the Brownian velocity in the equilibrium state became 2.0 μm s^{-1}, which was 88% of that of the fresh nanobeads. Similarly, when the anti-ORSV IgG-modified beads were stored for 12 months, the Brownian velocity became 6.2 μm s^{-1} in the equilibrium state. Thus, the results demonstrated that the analyte capturing ability of the antibody-modified nanobeads weakened during long-term storage.

Conclusions

In this study, an ORSV, one of the important orchid viruses, sensing technique based on the measuring nanobeads' Brownian velocity in real-time has been developed and characterized. Based on the results of the capsid protein sensing, a kinetic association model is established for analyzing the protein and antibody-coated nanobead binding rate in a free liquid space. The whole ORSV particle detection in plant sap prepared by PBS is also demonstrated. TEM images also validate the size and the shape changes of the nanobeads when binding with the ORSV. For testing the storage life, the nanobeads, stored up to 1 year since the modification with anti-ORSV onto them, can still be used to detect the ORSV.

Acknowledgements

This work is supported by the Ministry of Science and Technology of Taiwan under grant number MOST 100-2221-E-002-107-MY3. We would like to thank the facility support for microfabrication by the Nano-Electro-Mechanical-System (NEMS) research center, and TEM support by the Joint Center for Instruments and Researches, College of Bioresources and Agriculture, of National Taiwan University, Taiwan.

Notes and references

1 J. Findlay, W. Smith, J. Lee, G. Nordblom, I. Das, B. DeSilva, M. Khan and R. Bowsher, *J. Pharm. Biomed. Anal.*, 2000, **21**, 1249–1273.
2 G. Clarke, P. Elliott and C. Smaila, *Am. J. Reprod. Immunol. Microbiol.*, 1985, **7**, 118–123.
3 Y. Hokama, W. E. Takenaka, K. Nishimura, J. Ebesu, R. Bourke and P. K. Sullivan, *J. AOAC Int.*, 1997, **81**, 727–735.
4 E. Gorelik, D. P. Landsittel, A. M. Marrangoni, F. Modugno, L. Velikokhatnaya, M. T. Winans, W. L. Bigbee, R. B. Herberman and A. E. Lokshin, *Cancer Epidemiol., Biomarkers Prev.*, 2005, **14**, 981–987.
5 K. P. Chang, Y. T. Chang, C. C. Wu, Y. L. Liu, M. C. Chen, N. M. Tsang, C. L. Hsu, Y. S. Chang and J. S. Yu, *Head Neck*, 2011, **33**, 886–897.
6 F. Linkov, A. Lisovich, Z. Yurkovetsky, A. Marrangoni, L. Velikokhatnaya, B. Nolen, M. Winans, W. Bigbee, J. Siegfried and A. Lokshin, *Cancer Epidemiol., Biomarkers Prev.*, 2007, **16**, 102–107.
7 M. Arellano-Garcia, S. Hu, J. Wang, B. Henson, H. Zhou, D. Chia and D. Wong, *Oral Dis.*, 2008, **14**, 705–712.
8 Y. Murakami, T. Endo, S. Yamamura, N. Nagatani, Y. Takamura and E. Tamiya, *Anal. Biochem.*, 2004, **334**, 111–116.
9 R. Wacker, B. Ceyhan, P. Alhorn, D. Schueler, C. Lang and C. M. Niemeyer, *Biochem. Biophys. Res. Commun.*, 2007, **357**, 391–396.
10 J. E. Hardingham, D. Kotasek, R. E. Sage, M. C. Eaton, V. H. Pascoe and A. Dobrovic, *Mol. Med.*, 1995, **1**, 789.
11 A. Fan, C. Lau and J. Lu, *Anal. Chem.*, 2005, **77**, 3238–3242.
12 J. H. Thomas, S. K. Kim, P. J. Hesketh, H. B. Halsall and W. R. Heineman, *Anal. Chem.*, 2004, **76**, 2700–2707.
13 D. Holmes, J. K. She, P. L. Roach and H. Morgan, *Lab Chip*, 2007, **7**, 1048–1056.
14 Y. J. Fan, H. J. Sheen, Y. H. Liu, J. F. Tsai, T. H. Wu, K. C. Wu and S. Lin, *Langmuir*, 2010, **26**, 13751–13754.
15 V. M. Gorti, H. Shang, S. T. Wereley and G. U. Lee, *Langmuir*, 2008, **24**, 2947–2952.
16 Y. J. Fan, H. J. Sheen, C. J. Hsu, C. P. Liu, S. Lin and K. C. Wu, *Biosens. Bioelectron.*, 2009, **25**, 688–694.
17 Y.-J. Fan, H.-J. Sheen, Z.-Y. Chen, Y.-H. Liu, J.-F. Tsai and K.-C. Wu, *Microfluid. Nanofluid.*, 2015, DOI: 10.1007/s10404-015-1551-y.
18 S.-C. Lee and Y.-C. Chang, *Eur. J. Plant Pathol.*, 2008, **122**, 297–306.
19 F. Zettler, N. Ko, G. Wisler, M. Elliott and S. Wong, *Plant Dis.*, 1990, **74**, 621–626.
20 S. Wong, C. Chng, Y. Lee, K. Tan and F. Zettler, *Crop Prot.*, 1994, **13**, 235–239.
21 K. H. Ryu, W. M. Park, S. Y. Chung and K. E. Yoon, *Plant Dis.*, 1995, **79**, 321.
22 S. N. Chapman, in *Plant Virology Protocols*, ed. G. D. Foster and S. C. Taylor, Springer, New Jersey, 1998, pp. 123–129.
23 S. M. Rocha, L. A. Suzuki, A. D. T. Silva, G. C. Arruda and C. L. Rossi, *Rev. Inst. Med. Trop. Sao Paulo*, 2002, **44**, 57–58.
24 A. Einstein, *Ann. Phys.*, 1905, **17**, 549–560.
25 R. W. Glaser, *Anal. Biochem.*, 1993, **213**, 152–161.
26 S. W.-L. Tan, S.-M. Wong and R. M. Kini, *J. Virol. Methods*, 2000, **85**, 93–99.
27 W.-H. Chen and H.-H. Chen, *Orchid Biotechnology II*, World Scientific, 2011.

